sustainability

MDPI

Article

Rainfall-Conditioned Safety Screening of Mountain Nature-Based Recreation Spaces Under Relative Flash-Flood Potential in Guizhou, China

Qiang Hu [1], Xiangpeng Liang [1,*], Wenjing Si [2] and Yingyue Hou [2]

[1] College of Forestry, Xinyang Agriculture and Forestry University, Xinyang 464000, China
[2] College of Landscape Architecture and Art, Xinyang Agriculture and Forestry University, Xinyang 464000, China
* Correspondence: 2017290004@xyafu.edu.cn

Abstract

Mountain nature-based recreation spaces often combine high ecological quality with practical accessibility, yet they may also be constrained by sudden flash floods. Existing studies generally assess recreation opportunities and flood hazards separately, making it difficult to determine how potential recreation spaces progressively enter the scope of safety attention under different rainfall conditions. Taking Guizhou Province, China, as a case study, we developed history-informed standardised event-rainfall scenarios, assessed relative flash-flood potential using an NRCS-CN–HAND framework, and identified potential nature-based recreation opportunities from habitat quality and road proximity. We then analysed how areas requiring safety attention changed across rainfall conditions. The results show that the spatial extent of high relative flash-flood potential increased with event-total rainfall, but the rate of expansion varied markedly among rainfall stages, with the greatest province-wide expansion occurring between 30 and 40 mm. When potential recreation opportunities were intersected with high-potential areas, the resulting safety-attention areas expanded rapidly between 40 and 60 mm, with the largest increment between 40 and 50 mm. Activation rainfall for potential recreation opportunities was concentrated mainly between 50 and 70 mm and differed among prefecture-level units. By evaluating recreation opportunities and flash-flood constraints independently and linking them under comparable rainfall conditions, this study extends static recreation-opportunity mapping into dynamic safety screening and provides a practical spatial basis for prioritised site review, tiered inspection, and differentiated management of mountain nature-based recreation spaces.

Keywords: nature-based recreation; relative flash-flood potential; safety-attention areas; habitat quality; scenario analysis; spatial planning

Check for updates

Academic Editor: Dariusz Młyński

Received: 24 August 2026
Revised: 5 October 2026
Accepted: 8 October 2026
Published: 14 October 2026

Copyright: © 2026 by the authors. Licensee MDPI, Basel, Switzerland. This article is an open access article distributed under the terms and conditions of the Creative Commons Attribution (CC BY) license.

1. Introduction

In recent years, nature experiences, outdoor recreation, and mountain tourism have increasingly expanded into areas with high ecological quality and strong landscape appeal. Compared with urban parks and established tourist attractions, mountain nature-based recreation spaces are typically more dispersed and more dependent on linear access settings such as roads, valleys, and channels. Nature-based recreation is increasingly understood as a social–ecological system and an important cultural ecosystem service, while access to natural settings remains uneven across users and places [1–4]. At the same time, steep

terrain and short concentration times in mountain catchments can rapidly route surface runoff towards low-lying valleys and channels during heavy rainfall, meaning that access to some highly attractive natural spaces may also be limited by flash floods. Tourism development and land-use change can alter exposure patterns and amplify potential economic losses in mountain scenic areas [5], while event rainfall and rainfall duration have been used to identify flash-flood conditions at tourist attractions and to assess how those conditions may change under a changing climate [6]. Mountain recreation planning therefore needs to address not only where favourable recreation opportunities occur, but also when and to what extent these spaces become subject to flash-flood safety constraints under different rainfall conditions.

Assessments of nature-based recreation generally focus on ecological supply, landscape attractiveness, accessibility, and potential demand. A European-scale framework integrated natural supply, accessibility, and potential demand to assess outdoor recreation opportunities for land-use and regional planning [7], while work on urban and peri-urban recreational landscapes showed that the choice of distance metric and accessibility definition can materially affect planning outcomes [8]. Spatially explicit recreation research has since broadened to combine biophysical conditions with social-media information, accessibility, supply–demand relationships, and user preferences [9–14]. More recent studies have further linked recreation opportunities to spatial equity, regional supply–demand matching, tourism management, and planning [15–23]. Alongside these planning-oriented developments, recent methodological advances have increasingly incorporated machine-learning approaches into recreation assessment, including the use of social-media data, user-generated content, and citizen-science information to map recreation use and recreational ecosystem services [14,18,20]. In the ecologically fragile karst region of Guizhou, habitat quality and cultural-resource information have also been combined to identify potential tourism-development areas and differentiated conservation strategies [24]. These advances have moved recreation assessment from qualitative description towards spatially explicit identification, but most approaches still treat recreation opportunity as a relatively static spatial attribute and rarely ask whether the safety meaning of the same opportunity changes as rainfall conditions intensify.

Flash-flood research has developed along a largely separate technical pathway. Hydrodynamic and terrain-based approaches can represent flood processes and inundation patterns at catchment or site scales, while low-complexity HAND-based methods provide rapid spatial screening where the data are limited [15,25–29]. At broader scales, machine-learning and other data-driven susceptibility approaches, including deep-learning and explainable models, have increasingly been used to identify flood-prone areas and support disaster-management decisions [30–34]. Rainfall amount alone, however, does not determine flood response; storm organisation, rainfall-centre location, and terrain can substantially modify runoff concentration and peak-flow behaviour [35–40]. Existing approaches provide important foundations for local risk assessment and event warning, but studies concerning tourism commonly focus on individual scenic areas, specific events, or already defined exposure objects. For province-wide planning, a comparable framework is still needed to examine multiple rainfall levels under the same analytical rules and to determine how nature-based recreation opportunities progressively enter areas requiring safety attention as rainfall increases.

Guizhou is a mountainous karst province with abundant natural landscapes, and tourism and outdoor recreation depend strongly on mountain, valley, and waterside environments. Beyond established scenic areas, recreation may also occur in road-accessible forests, gorges, waterfalls, valleys, and peripheral spaces that are not fully represented by mapped tourism points of interest (POIs). Studies of ecosystem services, tourism ecolog-

ical adaptation, and spatial planning increasingly emphasise that ecological conditions, recreation uses, and development pressures should be represented explicitly rather than collapsed into a single undifferentiated suitability score [24,41–45]. If only formal attractions are treated as tourism-exposure objects, province-wide screening may omit potential recreation spaces that have both a natural basis and practical accessibility. Conversely, combining habitat quality, roads, tourism resources, and flash-flood constraints directly into one composite index would obscure the distinct meaning of ecological opportunity and safety limitation. For planning purposes, high habitat quality indicates a favourable ecological context; road proximity represents basic access opportunity; and flash-flood potential determines whether additional safety attention is warranted under a given rainfall pressure. Quantifying these dimensions separately before spatially coupling them therefore provides a clearer basis for identifying conflicts between ecological use and disaster safety.

To connect the identification of nature-based recreation opportunities with flash-flood safety assessment, this study uses event-total rainfall as a common comparison axis. Long-term rainfall information is used to position standardised main scenarios within the historical distribution, and the spatial responses of Guizhou Province and its nine prefecture-level units are repeatedly analysed within the same statistical framework. The hydrological component combines NRCS-CN event runoff, D8 routing, and HAND terrain constraints to construct high relative flash-flood potential and to describe how high-potential areas expand across rainfall conditions. The recreation component identifies potential nature-based recreation opportunity areas from habitat quality and road proximity, while tourism POIs are used to characterise the mapped formal-tourism context. A fixed potential scale is then used to calculate the minimum main-scenario rainfall at which each pixel first enters the high-potential class, and the overlap between high relative flash-flood potential and recreation opportunity areas is identified at each rainfall level to produce rainfall-conditioned safety-attention areas. Real-event replay is used as a supplementary check on whether the overall direction of scenario response persists under spatially heterogeneous rainfall.

Within this framework, the study addresses three questions: First, how do standardised event-total rainfall levels alter high relative flash-flood potential across Guizhou and its prefecture-level units, and does the expansion exhibit distinct stages and regional differences? Second, what proportion of potential nature-based recreation opportunity areas progressively enters the safety-attention state as rainfall increases, and how is the minimum activation rainfall distributed? Third, to what extent do mapped tourism POIs overlap these safety-attention areas, and do potential recreation spaces outside formal-tourism nodes also warrant planning review? The study develops a continuous analytical chain linking historical rainfall information, relative flash-flood potential, nature-based recreation opportunities, and dynamic safety-attention areas, thereby extending static resource identification into comparable rainfall-conditioned safety screening for mountain recreation planning, tiered inspection, and differentiated regional management in Guizhou.

2. Materials and Methods

2.1. Study Area

Guizhou Province is located in southwestern China and is characterised by pronounced topographic relief, widespread karst landforms, and a close spatial interweaving of mountain valleys and natural landscape resources (Figure 1). The study covers nine prefecture-level units: Guiyang, Zunyi, Liupanshui, Anshun, Bijie, Tongren, Qiandongnan, Qiannan, and Qianxinan. Based on the administrative boundary used here, Guizhou covers approximately 176,000 km^2. Because flash-flood generation and routing are not constrained by administrative boundaries, the hydrological computation domain was extended beyond

Guizhou to connected upstream hydrological areas. Runoff generation and routing were completed over this wider domain before results were clipped to the provincial boundary for analysis.

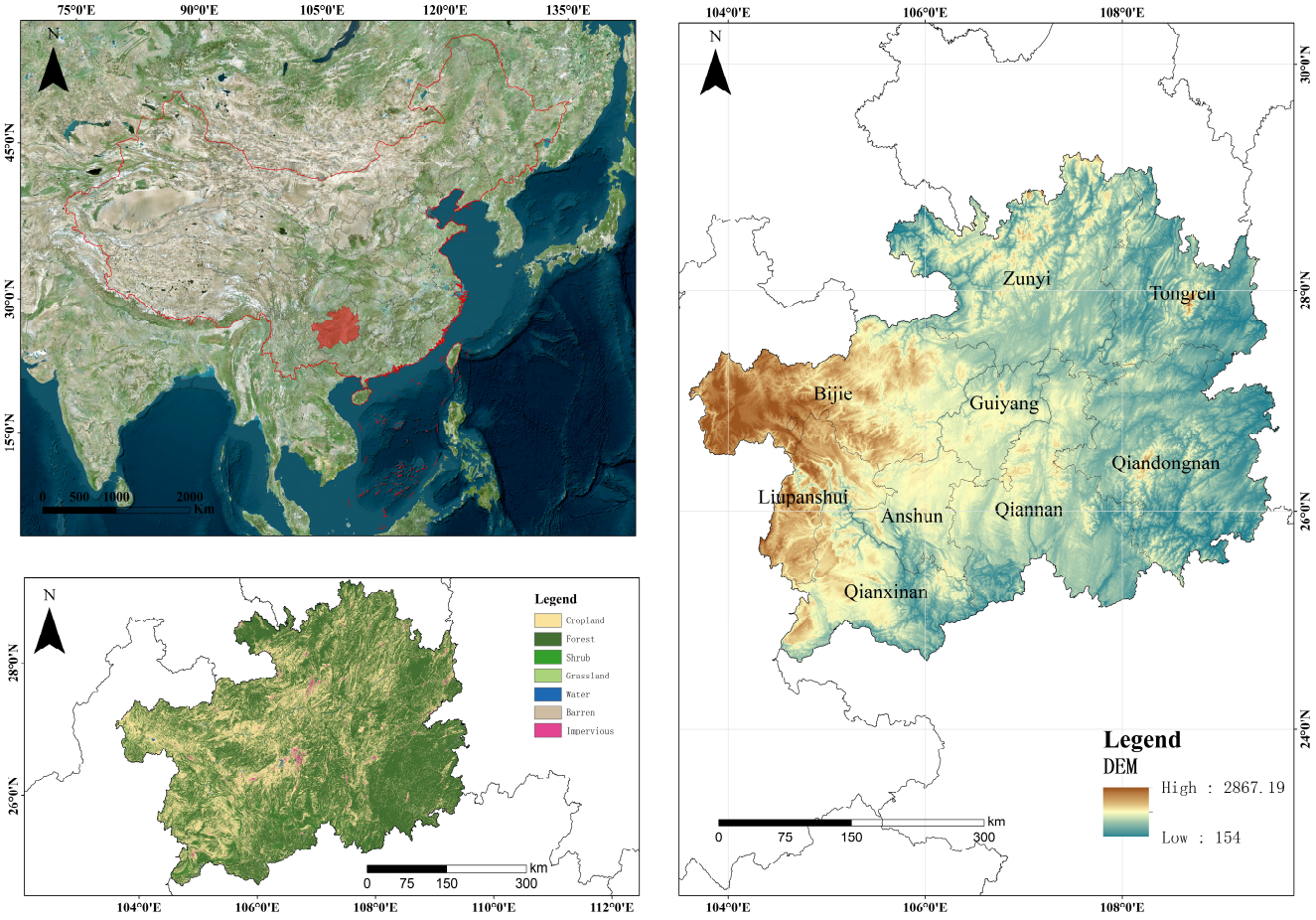


Figure 1. Study Area and Environmental Characteristics.

To ensure that ecological, hydrological, and recreational information could be compared on a common spatial basis, the final analysis used an Albers equal-area projection and a 250 m × 250 m regular grid. The effective hydrological analysis area within Guizhou was 176,075.44 km^2, while the jointly valid planning-analysis area for ecological background, roads, and flash-flood potential was 176,029.56 km^2. All prefecture-level comparisons used the same spatial base and statistical rules.

2.2. Data Sources and Preprocessing

The study integrated precipitation, land cover, hydrological soil groups, hydrotopographic information, ecological background, roads, tourism points of interest (POIs), and administrative boundaries (Table 1). Precipitation was derived from the half-hourly GPM IMERG V07 product (NASA Goddard Earth Sciences Data and Information Services Center (GES DISC), Greenbelt, MD, USA); warm-season data from 2001 to 2024 were used to construct the historical event-rainfall distribution, and 2025 data were used for real-event replay. IMERG V07 was recently evaluated over mainland China [46]. Land cover was represented by the 2025 CLCD 30 m product (Wuhan University, Wuhan, China), following the CLCD data lineage [47], and hydrological soil groups were represented by the approximately 250 m HYSOGs dataset [48]. Flow direction, HAND, and upstream area were derived from MERIT Hydro [27,49]. The ecological background was represented by the 2025 InVEST Habitat Quality output, (InVEST version 3.14.1; Natural Capital Project, Stanford

University, Stanford, CA, USA) an approach widely used to integrate habitat condition into ecosystem-service-based planning and tourism assessments [24,41]. Roads and tourism POIs represented the basic access conditions and the mapped formal-tourism context, respectively. Tourism POIs were derived from OpenStreetMap (OSM), with 4332 points retained within Guizhou under the documented category "POI (tourism attractions)". These POIs were used only to represent the mapped formal-tourism context rather than a complete inventory of tourism or recreation locations. No uniform independently verified positional-accuracy measure was available for all POIs.

Table 1. Main datasets and their roles in this study.

Data	Temporal and Spatial Information	Primary Use
GPM IMERG V07	Warm seasons, 2001–2025; 30 min; 0.1°	Historical rainfall distribution, standardised rainfall scenarios, and real-event replay
CLCD v01	2025; 30 m	Input to InVEST Habitat Quality and construction of CN parameters
HYSOGs	Static; approximately 250 m	Hydrological soil groups and CN parameter construction
MERIT Hydro	Static; 3 arc-sec	D8 routing, HAND constraint, and upstream-area stratification
InVEST Habitat Quality	2025; 30 m	Representation of ecological context
Guizhou Road Network	2025; vector	Distance to nearest road and basic access condition
OSM Tourism POIs	4332 points	Mapped formal-tourism context
Provincial- and Prefecture-Level Boundaries	Vector	Result clipping and prefecture-level statistics

Original GPM precipitation rates were converted to half-hourly rainfall depths and accumulated over each event window to obtain event-total rainfall. Continuous rasters were resampled using appropriate averaging or area-weighted procedures, while categorical data retained their class attributes. Hydrological routing was always undertaken on the native MERIT flow-direction grid. Final outputs were transformed to the 250 m equal-area grid for spatial overlay and area statistics. ArcGIS Desktop (version 10.8; Esri, Redlands, CA, USA) was used for spatial data processing and map preparation. The overall analytical framework is illustrated in Figure 2. The workflow links history-informed rainfall scenarios, hydrological response, nature-based recreation opportunities, rainfall-conditioned spatial coupling, and planning-oriented safety screening within a unified analytical structure.

2.3. History-Informed Rainfall Scenarios and Relative Flash-Flood Potential Assessment

Warm-season rainfall events were first identified from half-hourly GPM records for April–September 2001–2024. A time step was defined as a core rainfall time when the spatial P95 within Guizhou or the upstream computation domain reached 2 mm/30 min, or when the regional mean rainfall reached 0.4 mm/30 min. Adjacent core times separated by no more than 6 h were merged into one event. This procedure identified 1236 historical events, for which regional mean event-total rainfall was calculated separately for Guizhou and the upstream computation domain. Based on the historical empirical distribution, nine history-informed main scenarios were defined at 20, 30, 40, 50, 60, 70, 80, 90, and 100 mm/event, together with 150 and 200 mm/event stress scenarios. Each standardised scenario applied spatially uniform event-total rainfall across the full hydrological computation domain, thereby providing a directly comparable rainfall sequence. The uniform forcing was used deliberately as a controlled scenario design rather than as a reconstruction of individual

storms so that differences among scenarios primarily reflected changes in event-total rainfall. Spatial heterogeneity in real rainfall fields was evaluated separately through the 2025 event replays described below.

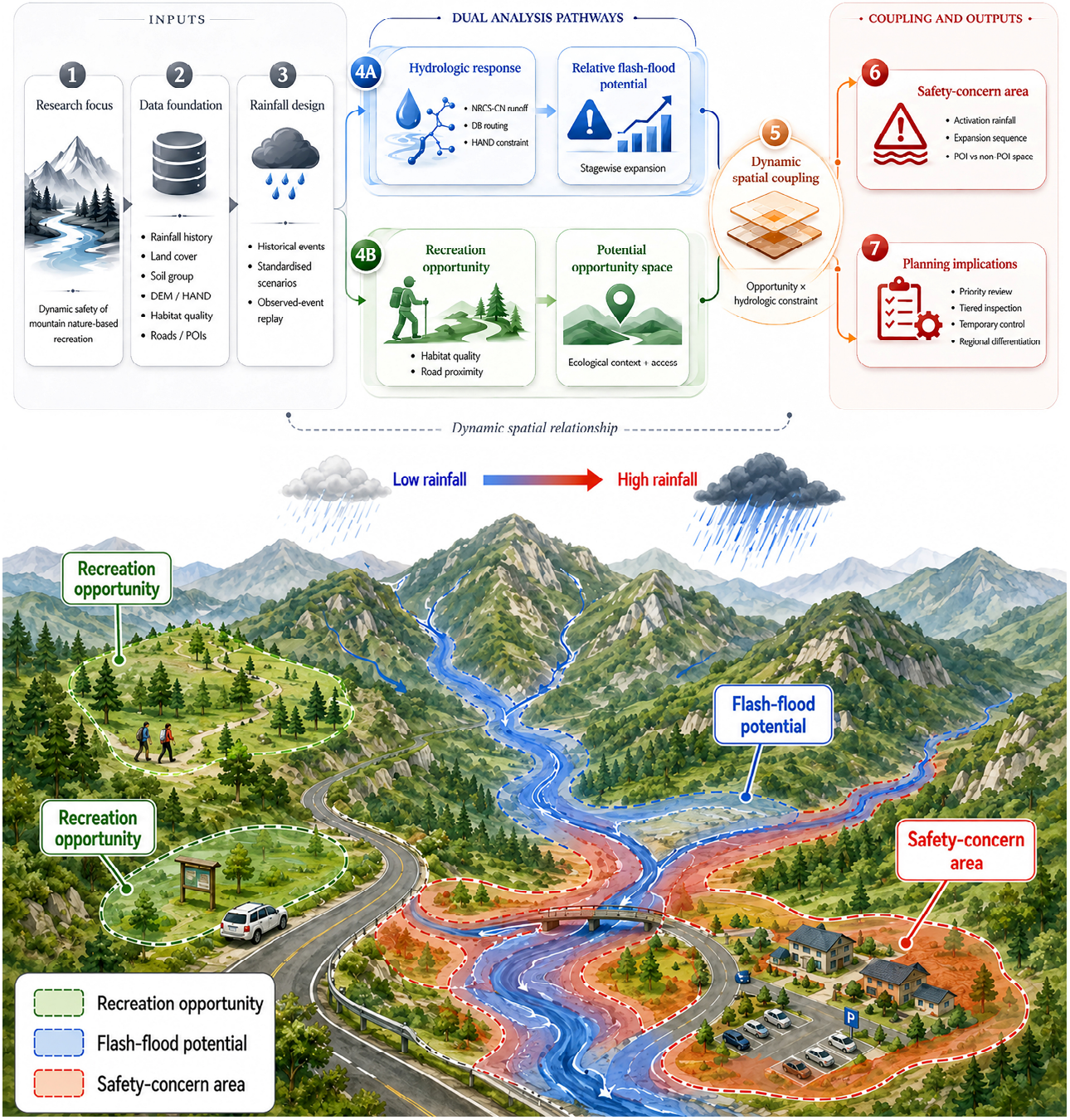


Figure 2. Analytical framework and conceptual representation of rainfall-conditioned safety screening for mountain nature-based recreation.

Event runoff was calculated using the NRCS-CN method. CN-II represents the average antecedent runoff condition in the NRCS-CN framework [50]. In the standardised rainfall scenarios, CN-II was used as a common baseline condition to keep antecedent runoff conditions consistent across scenarios so that differences among scenarios primarily reflected changes in event-total rainfall rather than differences in antecedent conditions. The principal CN-II values used in Table 2 were derived from the standard Curve Number tables in the USDA-NRCS *National Engineering Handbook*, Part 630—Hydrology, Chap-

ter 9: Hydrologic Soil-Cover Complexes [50]. Because this study used the 2025 CLCD land-cover classification, CLCD classes were matched to the closest corresponding NRCS land-use/cover categories according to their surface-cover characteristics, and CN-II values were assigned in combination with the HYSOGs dataset hydrologic soil groups A–D [48]. Cropland was represented by row crops under straight-row, good hydrologic condition; forest, shrubland, and grassland were matched to the corresponding woods, brush-dominated cover, and pasture/grassland categories; and barren land was represented by fallow–bare soil. Water and impervious surfaces were assigned CN = 98 following the NRCS guidance. Snow/ice and wetland had no direct corresponding entries in the adopted NRCS table and were therefore assigned CN = 98 as study-specific proxy values. These CLCD-to-NRCS correspondences represent study-specific parameterisation choices rather than an official NRCS mapping for CLCD classes. The resulting CN-II values are listed in Table 2. Potential maximum retention, S, was calculated as:

$$S = \frac{25,400}{CN} - 254 \quad (1)$$

Table 2. CN-II values by land-cover class and hydrological soil group based on the USDA-NRCS Curve Number framework [50].

Land-Cover Class	HSG A	HSG B	HSG C	HSG D
Cropland	67	78	85	89
Forest	36	60	73	79
Shrub	35	56	70	77
Grassland	49	69	79	84
Water	98	98	98	98
Snow/ice	98	98	98	98
Barren land	77	86	91	94
Impervious surface	98	98	98	98
Wetland	98	98	98	98

For a given event-total rainfall P, direct runoff depth R was calculated as:

$$R(P) = \begin{cases} 0, & P \leq 0.2S \\ \frac{(P-0.2S)^2}{P+0.8S}, & P > 0.2S \end{cases} \quad (2)$$

where P and R are both expressed in mm/event. To maintain water-volume consistency across grids, pixel runoff depth was converted to local runoff volume:

$$V = \frac{R\,A}{1000} \quad (3)$$

where A is the pixel area (m^2), and V is the runoff volume (m^3). Runoff volume was then mapped to the native MERIT grid and accumulated upstream along the D8 flow network. Relative flash-flood potential was constructed from accumulated runoff volume, upstream-area-normalised runoff and HAND. HAND provides a terrain-based measure of vertical position relative to the drainage network [27]. To reduce scale effects between large rivers and small catchments, valid pixels were stratified by upstream area into <10, 10–<100, 100–<1000, and ≥1000 km^2, and each component was standardised within its stratum using a common empirical distribution. Larger upstream runoff, larger accumulated runoff volume, and lower HAND all corresponded to greater relative flash-flood potential. The three standardised components were combined using an equal-weight geometric mean:

$$F(P) = \left(R_q\,R_v\,R_h\right)^{1/3} \quad (4)$$

where Rq, Rv, and Rh are the standardised ranks of upstream runoff, accumulated runoff volume, and HAND, respectively. Equal weighting was adopted as a neutral baseline because the three components represent complementary hydrological and topographic dimensions, which were transformed to a common standardised scale before aggregation [51]. In the absence of independent province-wide observations suitable for empirically calibrating component-specific weights, assigning unequal weights would introduce an additional subjective assumption. The equal-weight formulation therefore does not imply equal physical contributions of the three components, but provides a transparent and reproducible baseline for relative screening. To maintain comparability among rainfall scenarios, the reference scale was constructed once from the 20–200 mm simulation ensemble at 10 mm intervals and then held fixed for all scenarios and real-event replays. A fixed high-potential screening reference, T = 0.2616, was defined as the 60th percentile of pooled fixed-scale F values from five 2025 rainfall events for which complete pixel-level event-rainfall inputs and corresponding fixed-scale potential outputs were available and had passed temporal-completeness checks. The 2001–2024 historical ensemble and the 2025 application-year events served different purposes. The 1236 historical events were used to characterise the empirical distribution of regional event-total rainfall and to position the standardised rainfall scenarios within the long-term historical context; however, the archived historical workflow did not contain pixel-level event-rainfall fields and corresponding fixed-scale potential outputs for all historical events. By contrast, the five 2025 events had complete spatial event-rainfall inputs and corresponding potential outputs available under the 2025 application workflow, which was aligned with the 2025 land-cover parameterisation. Archived records retain the common event-detection and merging rules but do not document a reproducible ranking or sampling rule by which exactly these five events were selected from all 2025 candidates. They are therefore treated as an available application-year event set rather than as the five strongest events or a statistically representative sample of all storm types. Accordingly, T is interpreted as a sample-dependent fixed screening reference for scenario comparison rather than as a physically calibrated flood-occurrence threshold. For each pixel, the rainfall at which it first reached this threshold within the 20–100 mm main scenarios was defined as the main-scenario activation rainfall:

$$P_a = \min\{P{:}F(P) \geq T\} \quad (5)$$

Three 2025 events with different regional mean event-total rainfall amounts were further selected for replay: 7–8 June (22.24 mm), 26–28 May (50.57 mm), and 18–20 June (75.43 mm). Each real event used its spatially heterogeneous GPM accumulated-rainfall field, and relative flash-flood potential was calculated through the same runoff–routing–HAND chain used for the standardised scenarios. These replays were used to examine how the controlled scenario response differed under realistic spatially heterogeneous rainfall fields, including differences in rainfall-centre location. They were treated as a supplementary directional check rather than as an independent flood or hydrodynamic validation.

2.4. Identification of Potential Nature-Based Recreation Opportunity Areas

Nature-based recreation opportunity was identified based on two dimensions: ecological context and road-based access. Ecological context was represented by the InVEST Habitat Quality model, which was increasingly integrated into spatial planning and tourism-resource assessment [24,41]. Using 2025 CLCD as the land-cover base, impervious surfaces, barren land, and cropland were treated as the main threats, with threat intensity, maximum influence distance, and land-cover sensitivity considered jointly. Maximum influence distances were 8, 2, and 1 km for impervious surfaces, barren land, and cropland, respectively, with weights of 1.0, 0.4, and 0.7. Impervious surfaces used exponential decay,

whereas barren land and cropland used linear decay. Threat parameters are listed in Table 3, and habitat suitability and threat sensitivity by land-cover class are listed in Table 4.

Table 3. Threat parameters used in the InVEST Habitat Quality model.

Threat	Maximum Influence Distance (km)	Weight	Decay Type
Impervious surface	8.0	1.0	Exponential
Barren land	2.0	0.4	Linear
Cropland	1.0	0.7	Linear

Table 4. Habitat suitability and sensitivity to threats by land-cover class.

Land-Cover Class	Habitat Suitability	Impervious Surface	Barren Land	Cropland
Cropland	0.30	0.60	0.20	0.30
Forest	0.90	0.60	0.30	0.70
Shrub	0.80	0.60	0.30	0.70
Grassland	0.70	0.60	0.30	0.60
Water	0.80	0.50	0.20	0.70
Snow/ice	0.00	0.00	0.00	0.00
Barren land	0.10	0.10	0.00	0.10
Impervious surface	0.00	0.00	0.00	0.00
Wetland	0.90	0.70	0.30	0.70

The scaling parameter z was set to 2.5. A preliminary model run was conducted using k = 0.05 to obtain the maximum habitat-degradation value within Guizhou (Dmax); the half-saturation constant for the formal run was then set to k = 0.5Dmax. Habitat quality was expressed as:

$$Q = H\left(1 - \frac{D^z}{D^z + k^z}\right) \quad (6)$$

where Q is the habitat quality index; H is habitat suitability for the land-cover class; D is total degradation; k is the half-saturation constant; and z is the scaling parameter. The habitat-quality output was aggregated to 250 m, and a 9 × 9-cell neighbourhood mean was used to represent the surrounding ecological context. Basic road proximity was represented by Euclidean distance from each 250 m grid cell to the nearest road. This metric was used as a province-scale spatial proxy indicating proximity to the existing road network rather than as a behavioural measure of actual visitor accessibility. It does not account for slope, terrain barriers, trail connectivity, or actual travel time, and therefore should not be interpreted as representing real visitor movement routes or visitation intensity [8,16,17].

Within the jointly valid domain of habitat quality, road distance, and flash-flood potential, the 75th percentile of neighbourhood habitat quality (0.3497) was used to identify a relatively high ecological context, and a road distance of ≤1 km was used as the baseline basic road-proximity condition. These criteria were treated as relative province-scale screening conditions rather than fixed ecological or behavioural thresholds. Their intersection defined the potential nature-based recreation opportunity area, O:

$$O = I(Q \geq Q_{75}) \times I(D_r \leq 1000) \quad (7)$$

where I is an indicator function, and D_r is the distance to the nearest road. Accordingly, the resulting opportunity areas represent potential spatial conditions for nature-based recreation rather than observed visitor distribution or actual recreation-use intensity. Tourism POIs were not used to construct O; instead, distance to the nearest POI was used subsequently to describe the tourism context of opportunity areas and safety-attention areas.

2.5. Identification of Rainfall-Conditioned Recreation Safety-Attention Areas

High relative flash-flood potential under each rainfall scenario was overlaid with potential nature-based recreation opportunity areas to obtain rainfall-conditioned recreation safety-attention area C(P):

$$C(P) = O \times I(F(P) \geq T) \tag{8}$$

To compare responses among rainfall levels and prefecture-level units, the safety-attention ratio was calculated using potential nature-based recreation opportunity area as the denominator:

$$R_c(P) = \frac{A[C(P)]}{A(O)} \times 100\% \tag{9}$$

Province-wide and prefecture-level safety-attention areas and ratios were then calculated for each rainfall scenario, together with the activation rainfall at which opportunity pixels first entered the high-potential state. Areas within 2 km of the nearest tourism POI were treated as the baseline POI-proximate formal-tourism context, whereas areas >2 km from the nearest POI were treated as a non-POI-proximate context. This classification was used only to describe the composition of safety-attention areas under different mapped tourism contexts.

3. Results

3.1. Historical Rainfall Context and Province-Wide Relative Flash-Flood Response

A total of 1236 warm-season rainfall events were identified for 2001–2024. The Q75, Q90, Q95, and Q99 of regional mean event-total rainfall over Guizhou were 15.00, 28.06, 37.22, and 60.48 mm/event, respectively, with a historical maximum of 136.66 mm/event; corresponding Q99 and maximum values for the upstream computation domain were 25.02 and 49.41 mm/event (Figure 3a). Within the historical empirical distribution, the 20 mm main scenario corresponded to the 83.17th percentile for Guizhou and the 97.57th percentile for the upstream domain. The 50 mm scenario reached the 97.73rd percentile for Guizhou and was already at the upper end of the upstream-domain distribution. Main scenarios of 60–100 mm all lay in the high tail of the Guizhou historical distribution, while 150 and 200 mm were retained separately as stronger stress scenarios (Figure 3b).

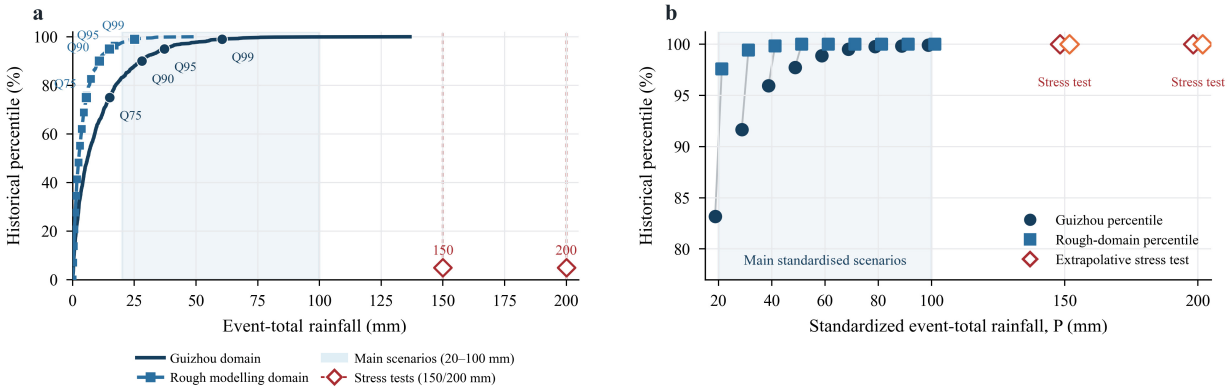


Figure 3. Historical rainfall context and standardised scenarios: (**a**) historical rainfall distributions and key quantiles; (**b**) historical positions of the standardised scenarios.

CN-II, local runoff, accumulated runoff volume, and HAND showed pronounced spatial differentiation. Under uniform rainfall forcing, local runoff varied with land cover and hydrological soil group; accumulated runoff progressively concentrated along river networks and valleys; and low HAND values were concentrated in valleys and low-lying

drainage settings (Figure 4a–d). Catchment area derived from the D8 routing network closely followed a 1:1 relationship with MERIT upstream area (Figure 4e).

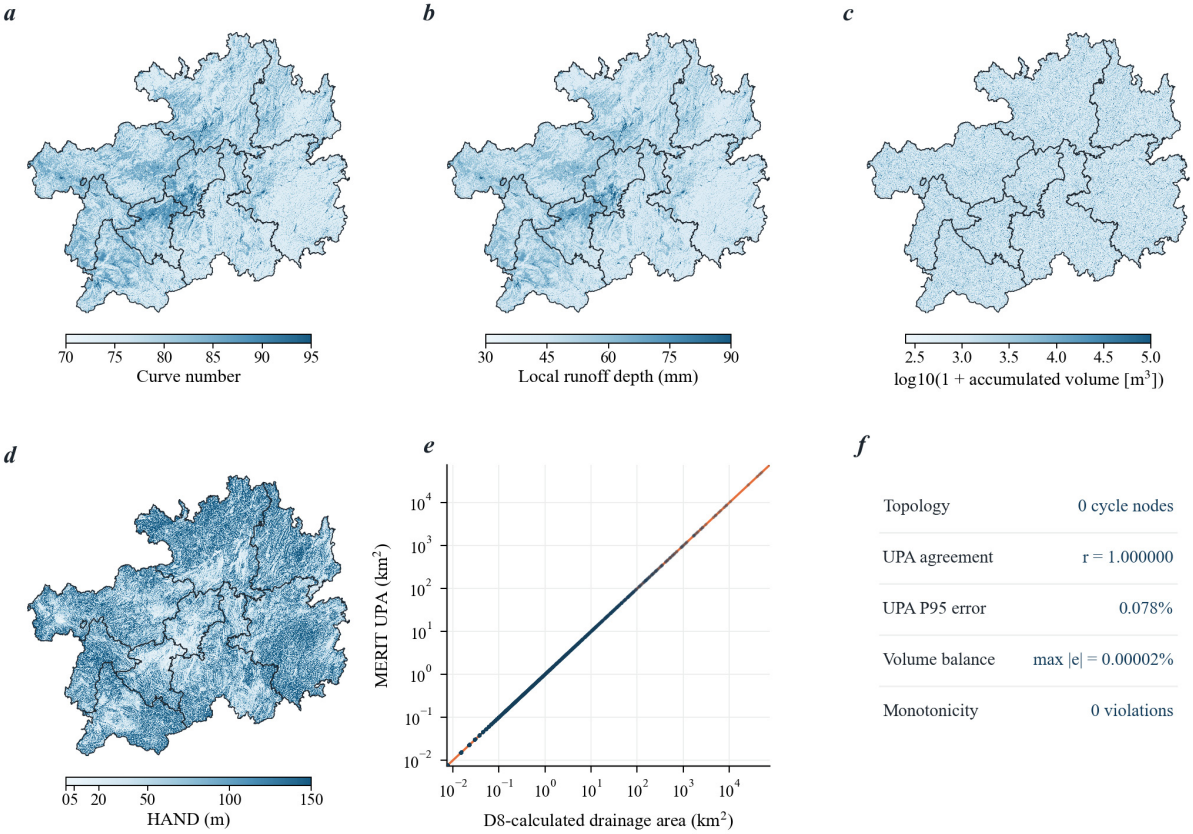


Figure 4. Hydrological inputs and computational validation: (**a**–**d**) CN-II, local runoff depth, accumulated runoff volume, and HAND; (**e**) D8–MERIT drainage-area comparison; (**f**) computational checks.

As event-total rainfall increased, high relative flash-flood potential expanded from localised patches and linear features into progressively more continuous areas (Figure 5). At 20 mm, the high-potential area was 1938.19 km^2, representing only 1.10% of the effective analysis area; this increased to 58,211.56 km^2 (33.06%) at 40 mm, 93,994.31 km^2 (53.38%) at 50 mm, and 160,281.12 km^2 (91.03%) at 100 mm. Incremental area between adjacent main scenarios first increased and then declined. The largest expansion occurred from 30 to 40 mm (+38,523.19 km^2), followed by 40–50 mm (+35,782.75 km^2). Subsequent increments progressively decreased, with only 4762.00 km^2 added from 90 to 100 mm. Under the 150 and 200 mm stress scenarios, the high-potential area reached 96.54% and 98.07% of the effective analysis area, respectively.

3.2. Prefecture-Level Differences, Activation Rainfall, and Real-Event Response

The proportion of high relative flash-flood potential increased with rainfall in all nine prefecture-level units, but differences were pronounced at low-to-intermediate rainfall levels (Figure 6a). At 40 mm, high-potential proportions were 49.6% in Guiyang and 48.2% in Anshun, compared with 39.6% in Bijie and 22.2% in Qiandongnan. At 50 mm, the values reached 70.3%, 66.6%, and 60.2% in Guiyang, Anshun, and Bijie, respectively, while Qiandongnan reached 43.6%. By 100 mm, every prefecture-level unit exceeded 87%, with 97.4% in Guiyang, 95.2% in Anshun, 93.9% in Qiannan, and 87.7% in Zunyi.

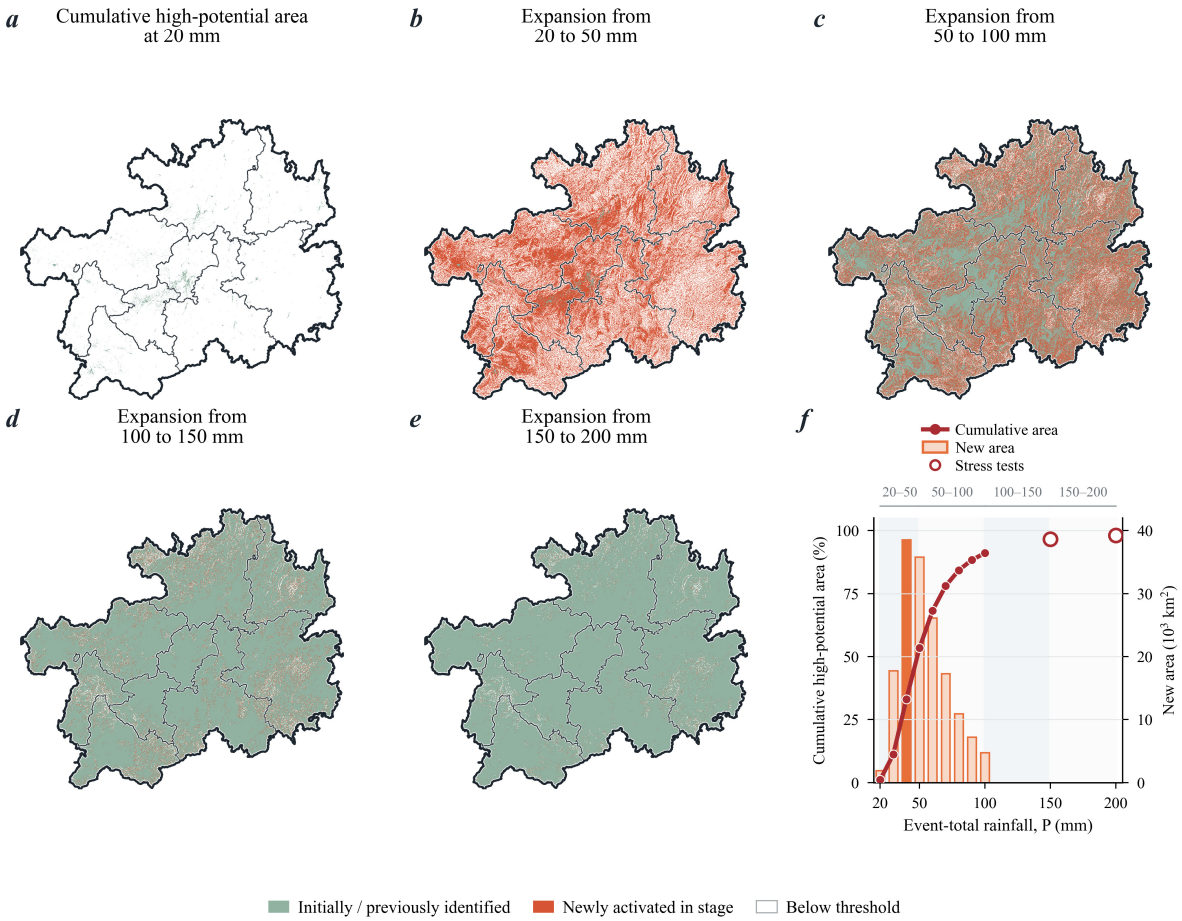
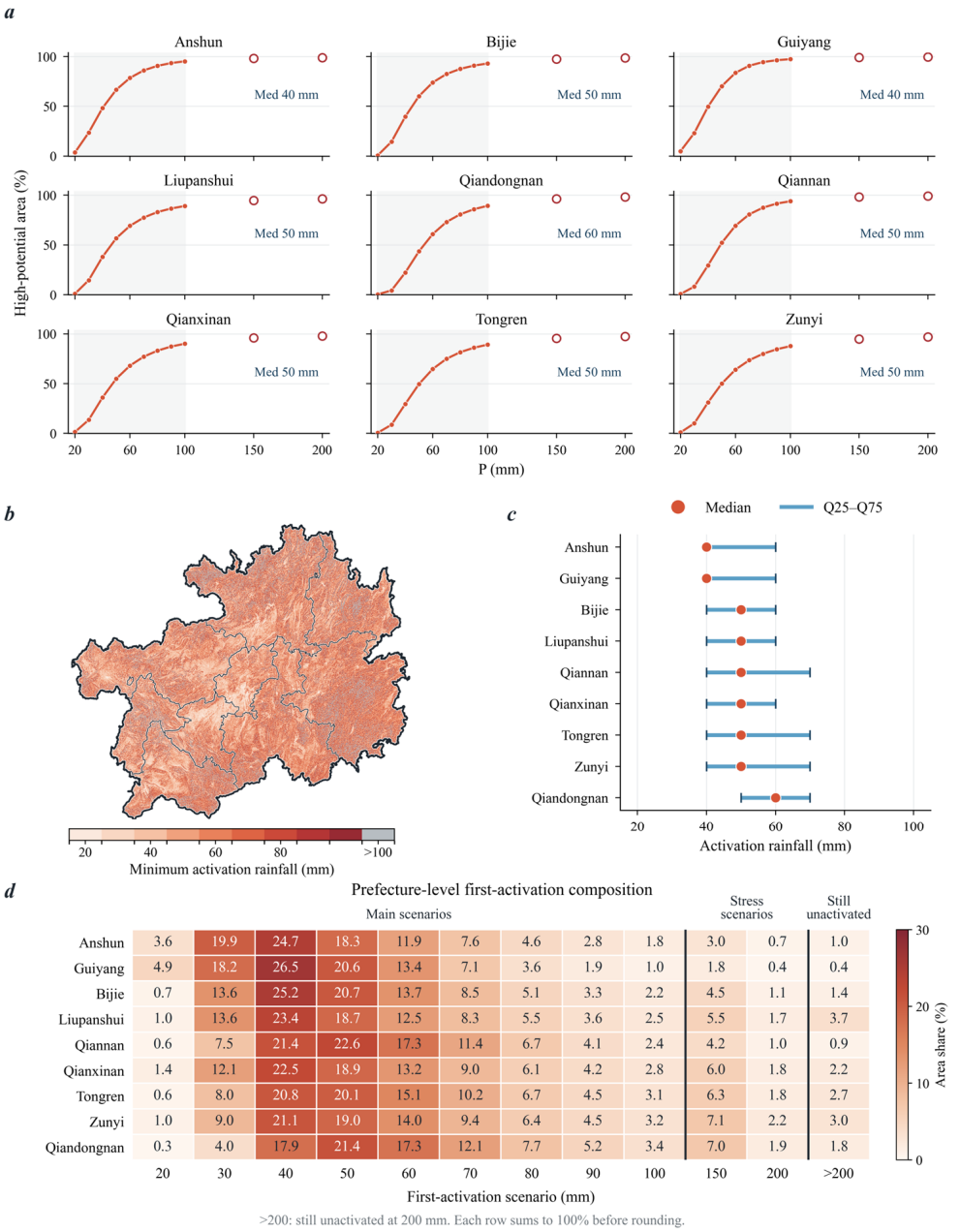


Figure 5. Rainfall-driven expansion of high relative flash-flood potential: (**a**) cumulative high-potential area at P = 20 mm; (**b**–**e**) previously identified and newly added high-potential areas during the 20–50, 50–100, 100–150, and 150–200 mm stages, respectively; (**f**) province-wide cumulative response and incremental expansion.

Main-scenario activation rainfall further revealed spatial differences among prefecture-level units (Figure 6b,c). Median activation rainfall was 40 mm in Guiyang and Anshun; 50 mm in Bijie, Liupanshui, Qiannan, Qianxinan, Tongren, and Zunyi; and 60 mm in Qiandongnan. Across Guizhou, 8.97% of the effective analysis area did not reach the high-potential threshold within the 20–100 mm main-scenario range. Prefecture-level proportions ranged from 2.64% to 12.29%, with the lowest value in Guiyang and the highest in Zunyi (Figure 6d).

The three representative 2025 events showed a consistent increase in high-potential area with increasing regional event-total rainfall under their observed spatial rainfall fields (Figure 7). For the 7–8 June event, regional mean event-total rainfall over Guizhou was 22.24 mm, and the high-potential area was 31,788.12 km^2 (18.05%). For 26–28 May, event-total rainfall was 50.57 mm, and the high-potential proportion reached 50.86%. For 18–20 June, event-total rainfall was 75.43 mm, and the high-potential area reached 117,515.75 km^2 (66.74%). Thus, the overall high-potential extent increased with event rainfall, while event-specific spatial differences associated with different rainfall centres remained evident.



	20	30	40	50	60	70	80	90	100	150	200	>200
Anshun	3.6	19.9	24.7	18.3	11.9	7.6	4.6	2.8	1.8	3.0	0.7	1.0
Guiyang	4.9	18.2	26.5	20.6	13.4	7.1	3.6	1.9	1.0	1.8	0.4	0.4
Bijie	0.7	13.6	25.2	20.7	13.7	8.5	5.1	3.3	2.2	4.5	1.1	1.4
Liupanshui	1.0	13.6	23.4	18.7	12.5	8.3	5.5	3.6	2.5	5.5	1.7	3.7
Qiannan	0.6	7.5	21.4	22.6	17.3	11.4	6.7	4.1	2.4	4.2	1.0	0.9
Qianxinan	1.4	12.1	22.5	18.9	13.2	9.0	6.1	4.2	2.8	6.0	1.8	2.2
Tongren	0.6	8.0	20.8	20.1	15.1	10.2	6.7	4.5	3.1	6.3	1.8	2.7
Zunyi	1.0	9.0	21.1	19.0	14.0	9.4	6.4	4.5	3.2	7.1	2.2	3.0
Qiandongnan	0.3	4.0	17.9	21.4	17.3	12.1	7.7	5.2	3.4	7.0	1.9	1.8

Figure 6. Prefecture-level responses and activation rainfall: (**a**) high-potential response curves; (**b**) spatial distribution of activation rainfall; (**c**) medians and Q25–Q75; (**d**) prefecture-level first-activation composition across the main and stress scenarios, including areas remaining unactivated at 200 mm.

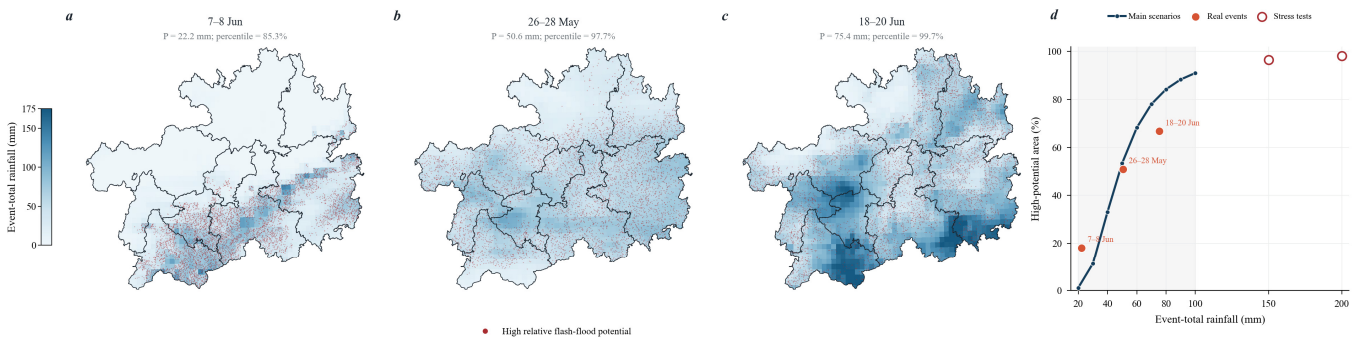


Figure 7. Real-event replay and standardised scenario comparison: (**a**–**c**) events of 7–8 June, 26–28 May, and 18–20 June 2025; (**d**) comparison with the standardised scenario response.

3.3. Spatial Characteristics of Potential Nature-Based Recreation Opportunity Areas

Neighbourhood habitat quality and road-based access showed pronounced spatial differentiation across Guizhou (Figure 8a,b). Relatively high ecological-context areas covered 44,007.44 km^2, or 25.00% of the jointly valid analysis domain, while areas within 1 km of a road covered 98,293.06 km^2, or 55.84%. Their intersection yielded 13,334.19 km^2 of potential nature-based recreation opportunity area, equivalent to 7.57% of the jointly valid domain, with an overall patchy and banded spatial pattern (Figure 8c).

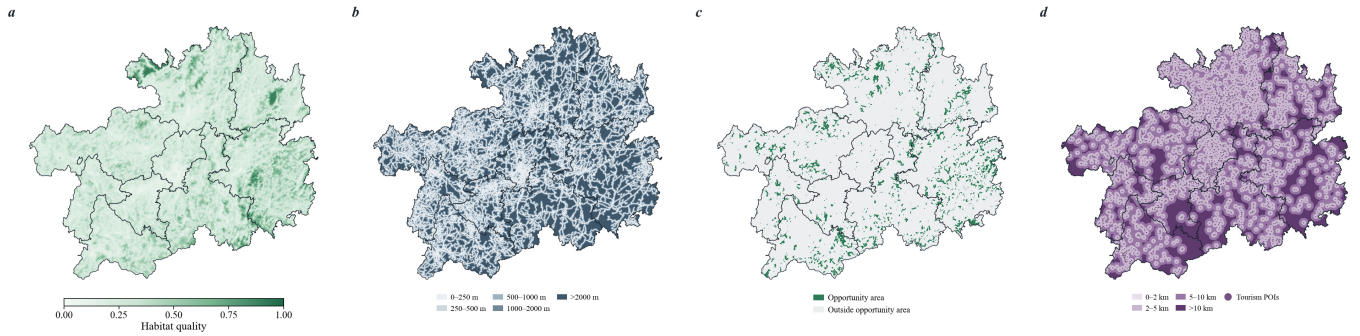


Figure 8. Nature-based recreation opportunity and tourism context: (**a**) habitat quality; (**b**) road distance; (**c**) recreation-opportunity area; (**d**) tourism-POI context.

Potential nature-based recreation opportunity areas varied substantially among prefecture-level units. Qiandongnan had the largest area, 3570.69 km^2 (11.80% of its effective domain), followed by Qianxinan with 1643.75 km^2 (9.78%). Qiannan, Zunyi, and Bijie contained 1969.75, 2136.88, and 1941.06 km^2, respectively. Guiyang contained only 114.25 km^2 (1.42%). A total of 4332 tourism POIs were mapped across the province, including 1073 in Guiyang and 972 in Zunyi. POI distribution and potential recreation opportunity showed different regional combinations (Figure 8d).

3.4. Rainfall-Conditioned Nature-Based Recreation Safety-Attention Areas

Nature-based recreation safety-attention areas expanded continuously as event-total rainfall increased (Figure 9a). At 20 mm, the area was only 3.44 km^2, equivalent to 0.03% of the potential recreation opportunity area. It increased to 2360.69 km^2 (17.70%) at 40 mm, 4975.44 km^2 (37.31%) at 50 mm, 8927.81 km^2 (66.95%) at 70 mm, and 11,492.25 km^2 (86.19%) at 100 mm. The largest 10 mm increment occurred from 40 to 50 mm (+2614.75 km^2); a further 2246.75 km^2 was added from 50 to 60 mm, after which increments progressively declined. Under the 150 and 200 mm stress scenarios, safety-attention ratios reached 94.82% and 97.26%, respectively.

Safety-attention ratios increased in all prefecture-level units, although expansion rates differed (Figure 9b). At 50 mm, Bijie, Guiyang, and Anshun reached 43.1%, 41.3%, and 41.1%, respectively, compared with 33.2% in Tongren and 33.7% in Zunyi. At 100 mm, Guiyang reached 93.8%, Qiannan and Bijie reached 90.0% and 89.6%, respectively, and Tongren and Zunyi reached 80.6% and 80.5%. Across all potential recreation opportunity areas, the Q25, median, and Q75 of activation rainfall were 50, 60, and 70 mm, respectively, while 13.81% of the opportunity area had not entered the safety-attention state by the 100 mm main scenario (Figure 9c).

In relation to mapped tourism POIs, safety-attention areas were concentrated mainly beyond the POI-proximate context. At 100 mm, 898.62 km^2 of safety-attention area lay within 2 km of a tourism POI, compared with 10,593.62 km^2 beyond 2 km; the POI-proximate component therefore represented 7.82% of the total. Under the 200 mm stress scenario, the corresponding proportion was 7.91%. Maps of representative rainfall stages

further showed safety-attention areas expanding from localised patches at 40 mm to progressively wider extents at 50, 70, and 100 mm (Figure 9d).

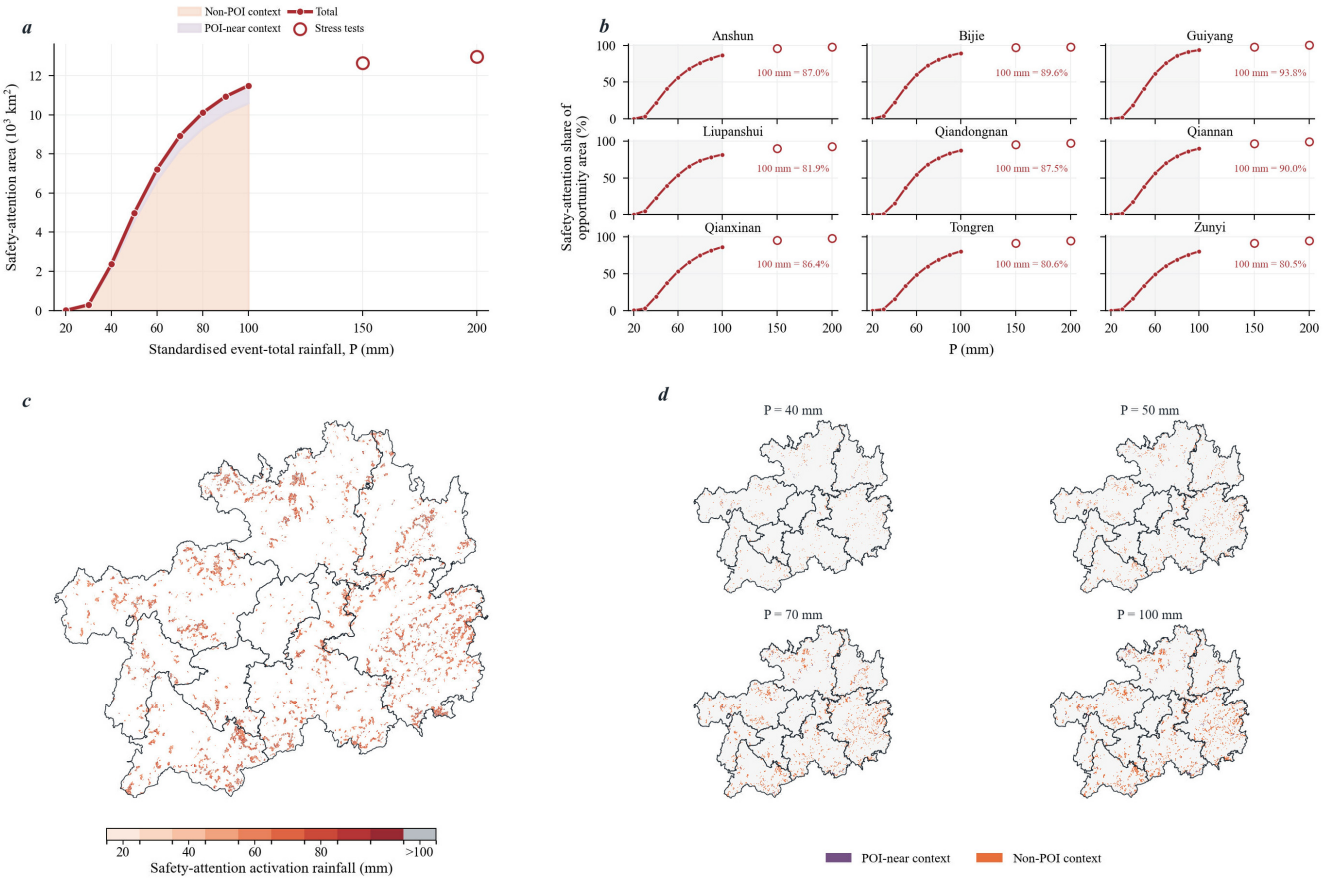


Figure 9. Rainfall-conditioned safety-attention areas: (**a**) province-wide response; (**b**) prefecture-level responses; (**c**) activation rainfall; (**d**) spatial patterns at P = 40, 50, 70, and 100 mm.

4. Discussion

The central contribution of this study is not a one-off spatial overlay of recreation opportunity and flash-flood potential, but an examination of how their relationship changes with rainfall conditions. Taken together, the results support a broader interpretation: mountain nature-based recreation spaces do not possess a fixed safety status; rather, their planning significance depends on the dynamic spatial relationship between recreation opportunity and flash-flood hydrological constraints under changing rainfall conditions. In other words, ecological context and basic access determine where recreation may be possible, whereas rainfall conditions and the corresponding flash-flood potential determine when those spaces warrant safety attention. This perspective provides a common logic for interpreting the rapid expansion of flash-flood potential at 30–40 mm, the largest increase in recreation safety-attention area at 40–50 mm, and the concentration of activation rainfall at 50–70 mm. It therefore shifts the discussion from explaining individual results towards understanding how recreation opportunities interact with hydrological constraints.

4.1. From Static Opportunity Identification to Dynamic Safety Assessment

Nature-based recreation assessments generally focus on ecological supply, landscape attractiveness, accessibility, and potential demand, with the primary aim of identifying areas of relatively high recreation value or development potential [7,10,11,21,23,24]. These approaches provide an important basis for resource conservation and recreation planning, but their outputs are essentially spatial assessments of opportunity under relatively stable

background conditions. Flash-flood research, by contrast, commonly evaluates changing hazard conditions for specific events, catchments, or tourist sites using hydrological–hydrodynamic simulation, rainfall thresholds, or susceptibility mapping [5,6,30]. When these two lines of research remain separate, whether a place is "suitable for recreation" and whether it "requires safety attention" can easily be treated as two fixed spatial attributes. Our results show that this assumption is inadequate in mountain environments. The potential recreation-opportunity layer remains unchanged across the standardised scenarios, whereas the proportion entering the safety-attention state changes markedly with event-total rainfall. Safety is therefore not an inherent and invariant property of recreation opportunity space; its planning meaning changes as external hydrological conditions change.

This distinction also explains why mountain recreation planning should not rely solely on a composite suitability score. Relatively high habitat quality and road proximity represent recreation opportunity, whereas flash-flood potential represents a hydrological constraint under a given rainfall condition; the two dimensions play fundamentally different roles in planning decisions. Combining them through a single weighted score could allow favourable ecological conditions to compensate mathematically for strong hydrological constraints, thereby obscuring locations that warrant safety review. Evaluating the two dimensions independently and then identifying their overlap under a common rainfall sequence distinguishes, for example, areas with recreation opportunity but currently weak hydrological constraints from areas with recreation opportunity that have already entered a high-potential state. Relative to approaches that mainly answer where recreation opportunities occur, this framework additionally asks under what conditions the same opportunity space acquires a different safety meaning. It therefore extends recreation-space assessment from static resource identification towards dynamic safety assessment under changing environmental conditions.

4.2. Stage Differences Between Hydrological-Potential Expansion and Planning Attention

The different expansion stages of province-wide high relative flash-flood potential and recreation safety-attention areas provide the clearest evidence of this dynamic relationship. The largest 10 mm increase in high-potential area across Guizhou occurred from 30 to 40 mm, whereas after high-potential areas were intersected with potential nature-based recreation opportunities, the safety-attention area expanded rapidly from 40 to 60 mm and showed its largest increment from 40 to 50 mm. The first process describes the outward expansion of hydrological constraints across the province; the second depends on whether new high-potential locations actually enter the fixed distribution of recreation opportunities. Consequently, a rapid increase in flash-flood potential does not translate automatically or proportionally into an equivalent increase in planning-relevant safety-attention area. Hydrological change becomes a recreation-planning issue only where it overlaps spaces that already possess recreation opportunity.

The difference between the 30–40 mm and 40–50 mm maximum-increment intervals should therefore not be interpreted as a fixed "10 mm lag". Rather, the two intervals refer to different spatial objects and different analytical questions: the former identifies when high relative flash-flood potential expands most rapidly across the whole province, whereas the latter identifies when the greatest amount of that expansion enters potential recreation space. This distinction prevents "more flash-flood potential" from being treated as synonymous with "a proportionally greater recreation-safety problem". For planning, the more informative question is when hydrological constraints begin to overlap recreation opportunities at a scale sufficient to alter management priorities. This differentiates the hydrological response from the planning response without implying a causal or operational rainfall threshold.

Activation rainfall further reveals the spatial differentiation of this relationship. Activation rainfall for potential recreation opportunities was concentrated mainly between 50 and 70 mm and varied substantially among prefecture-level units, indicating that spaces with similar recreation-opportunity status do not enter the high relative flash-flood-potential state under the same rainfall condition. Here, activation rainfall is neither a critical rainfall for actual flash-flood occurrence nor an operational warning threshold. Likewise, the fixed T value is a framework-specific screening reference rather than a universally transferable flood threshold; its numerical value should be re-established when the framework is applied under different land-cover conditions, regions, or modelling settings. In addition, because the present T value was derived from a limited five-event 2025 application-year set rather than from a complete historical spatial-event ensemble, its numerical value should be regarded as sample-dependent rather than as a long-term climatological or operational threshold. It is the position within a common scenario sequence at which a location first reaches the fixed high-potential criterion. Its planning value lies in converting a static question—whether a place warrants attention—into a comparable conditional question—under what rainfall condition it should be prioritised. This is consistent with the broader principle that tourism and recreation planning should respond to regional differences rather than impose uniform strategies [16,24,52], while showing that such differences arise not only from resource endowment but also from the way recreation opportunities and hydrological constraints combine under changing rainfall conditions.

The three 2025 real-event replays provide a real-world reference for the standardised scenarios. As regional mean event-total rainfall increased, the overall extent of high relative flash-flood potential also increased, but the observed events did not fall exactly on the uniform-rainfall response curve. Rainfall-centre location, storm spatial organisation, and their relationship with basin morphology can alter runoff generation and concentration [36–38,40]. Standardised scenarios and real-event replays should therefore be viewed as complementary rather than interchangeable. For this reason, the standardised uniform-rainfall sequence was retained as the primary comparison axis rather than being replaced by multiple spatial rainfall patterns, which would simultaneously vary rainfall amount and spatial organisation and thereby reduce direct comparability among scenarios. The former provides controlled conditions for establishing a directly comparable rainfall–spatial-response relationship, whereas the latter provides an event-specific reference showing how the spatial response may differ under heterogeneous real-event rainfall forcing. Their combination allows stage-dependent patterns to be identified without mistaking scenario positions for actual flash-flood occurrence thresholds.

4.3. Planning Implications and Scope of Dynamic Safety Identification

The most direct planning implication is that mountain recreation safety should not be represented only by a single fixed zoning map. Instead, the spatial extent requiring attention can be allowed to expand progressively with rainfall conditions. Opportunity areas with lower activation rainfall and earlier entry into the high-potential state can be prioritised for field review of valleys, road-adjacent spaces, recreation nodes, and associated facilities; as rainfall conditions intensify, inspection and temporary management can then be extended according to the expansion of safety-attention areas. Accordingly, activation rainfall should be used to rank locations by their relative priority within the standardised scenario system, rather than by directly comparing values such as 50–70 mm with observed or forecast rainfall to trigger operational warnings; any real-time warning threshold would require separate local calibration and validation using observed hydrometeorological and flood information. Differences among prefecture-level units further indicate that a common province-wide rainfall sequence is useful as a comparison benchmark, but it should not

imply identical spatial management priorities in all regions. The planning focus thus shifts from a one-off classification of "safe" and "unsafe" areas towards identifying which spaces should be reviewed first and which should enter the scope of attention only under stronger rainfall conditions.

The tourism-POI analysis further shows that province-wide safety screening should not be confined to formal scenic areas. At 100 mm, the 2 km POI-proximate context accounted for only 7.82% of total safety-attention area, indicating that mapped tourism nodes represent only part of the potential recreation domain. In a mountainous province such as Guizhou, road-accessible forests, gorges, valleys, waterfall surroundings, and areas outside established scenic sites may also provide nature-based recreation opportunities. Province-wide screening should therefore extend beyond formal-tourism nodes to potential recreation spaces with a favourable ecological context and basic road proximity, after which user-generated social-media data, visitor-activity records, and field surveys can be incorporated to validate actual recreation use and distinguish frequently used sites from areas that represent only potential opportunities. Recent recreation studies increasingly demonstrate the value of user-generated content, citizen science, and spatial modelling for representing recreation use beyond formal facilities [1,13,14,18–20]. In this study, the role of POIs is, therefore, to contextualise formal-tourism space rather than to define recreation opportunity itself.

The framework is intended for province-scale screening rather than fine-scale flood prediction. Standardised event-total rainfall preserves direct comparability across scenarios, but real flash floods are additionally influenced by rainfall duration, within-event intensity, antecedent wetness, and storm location [6,38,40]. The NRCS-CN, D8-routing, and HAND components provide an efficient representation of relative flash-flood potential over large areas, but they do not directly estimate flood depth, velocity, arrival time, or precise inundation boundaries. Accordingly, detailed flood depth and arrival time should be evaluated at priority sites through local hydrodynamic modelling combined with flood-mark, water-level, or other event-based observations. HAND-based methods also remain sensitive to terrain resolution, hydro-conditioning, and drainage representation [15,25,26,28,29]. Because component-specific weights were not empirically calibrated, we further tested three symmetric alternative weighting schemes. All tested schemes retained increasing high-potential extent from 20 to 50 to 100 mm, although absolute extent and local spatial boundaries varied; the equal-weight formulation should therefore be interpreted as a transparent baseline screening configuration rather than a uniquely optimal weighting scheme. Additional uncertainty arises from satellite rainfall retrieval and CN-II parameterisation, for which province-wide event-specific runoff observations suitable for calibration are unavailable. The sensitivity analyses showed that absolute activation-rainfall values and mapped extents varied under alternative screening settings, whereas the progressive rainfall-response pattern and the broad historical positioning of the standardised scenarios were retained across the tested alternatives; these tests therefore provide a bounded robustness assessment rather than a complete probabilistic uncertainty envelope. Likewise, Euclidean distance to the road network represents only basic road proximity and cannot substitute for behaviourally realistic accessibility based on travel time, slope, terrain barriers, trail connectivity, or visitor movement. Incorporating these factors would be more appropriate in subsequent local-scale assessments once sufficiently detailed trail and movement data are available. Cross-regional application also requires local adaptation because soil hydrological properties can alter CN-based runoff response, terrain and drainage characteristics can affect HAND representation and flow concentration, and local recreation patterns can influence the identification of potential recreation opportunities; the corresponding inputs and screening criteria should therefore

be re-parameterised for each target region. A more appropriate application pathway is, therefore, to use the present framework first to identify low-activation-rainfall and high-attention areas at the provincial scale, and then concentrate higher-resolution topography, flood marks, water-level observations, two-dimensional hydrodynamic modelling, and observed recreation-use data on those priority locations. This retains the efficiency of broad-area comparison while defining clear targets for subsequent local validation.

5. Conclusions

This study evaluated potential nature-based recreation opportunities and relative flash-flood potential independently and examined how their spatial relationship changes across a common sequence of event-total rainfall scenarios in Guizhou Province. The results show that mountain nature-based recreation spaces do not possess a fixed safety status; rather, their planning significance depends on the dynamic spatial relationship between recreation opportunities and flash-flood hydrological constraints under different rainfall conditions. The largest province-wide 10 mm increment in high relative flash-flood potential occurred from 30 to 40 mm, whereas the largest increase in recreation safety-attention area occurred from 40 to 50 mm. Thus, rapid expansion of hydrological potential does not translate synchronously into an equivalent planning-attention response; it becomes planning-relevant only where newly intensified hydrological constraints enter potential recreation space. Activation rainfall for potential recreation opportunities was concentrated mainly between 50 and 70 mm and showed clear prefecture-level differences, further demonstrating that different locations enter the safety-attention domain under different conditions and in different sequences.

Accordingly, this study advances the planning question from "where are recreation opportunities located?" to "under what rainfall conditions should particular recreation opportunities be prioritised for safety attention?" By retaining recreation opportunity and hydrological constraints as distinct spatial information and converting their overlap under a common rainfall sequence into comparable dynamic screening information, the framework can support prioritised site review, comparison among prefecture-level units, tiered inspection, and differentiated management. The POI analysis also indicates that province-wide safety governance should not be restricted to formal-tourism nodes but should extend, at the screening stage, to potential recreation spaces with a favourable ecological context and basic road proximity. Activation rainfall and stage-dependent results are relative response positions within the standardised Guizhou scenario system and should not be interpreted as operational warning thresholds or fixed parameters transferable to other regions. The framework is best used as a province-scale first-stage screening tool, followed by local refinement using more detailed hydrological and recreation-use information.

Author Contributions: Q.H.: Conceptualisation, investigation, visualisation, writing—review and editing, formal analysis, funding acquisition; X.L.: Conceptualisation, supervision, writing—review and editing; W.S.: Investigation; Y.H.: Investigation, funding acquisition. All authors have read and agreed to the published version of the manuscript.

Funding: This work was supported by the Key Scientific Research Project of Higher Education Institutions of Henan Province (Grant/Award Number: 24A220005); the Soft Science Research Project of Henan Province (Grant/Award Number: 262400411081); and the Soft Science Research Program of Xinyang City (Grant/Award Number: 20250049).

Institutional Review Board Statement: Not applicable.

Informed Consent Statement: Not applicable.

Data Availability Statement: The datasets used in this study are derived from publicly available sources and processed/generated datasets. The precipitation data were obtained from the Global Precipitation Measurement (GPM) Integrated Multi-satellite Retrievals for GPM (IMERG) Version 07 dataset. Land-cover data were obtained from the China Land Cover Dataset (CLCD), hydrological soil group data from the HYSOGs 250m dataset, and hydro-topographic data from the MERIT Hydro dataset. The ecological habitat quality data were generated using the InVEST Habitat Quality model based on publicly available land-cover and environmental datasets. The processed datasets generated during this study—including historical rainfall event datasets, standardised rainfall scenario datasets, relative flash-flood potential outputs, activation rainfall maps, and rainfall-conditioned safety-attention area datasets—are available from the corresponding author upon reasonable request.

Acknowledgments: The authors gratefully acknowledge the developers and providers of the GPM IMERG, CLCD, HYSOGs, MERIT Hydro, and InVEST datasets and tools that supported this study.

Conflicts of Interest: The authors declare no conflicts of interest.

References

1. Groulx, M.; Wigglesworth, J.; DeLorey, R.; Harris, N.; Harris, P.; Lamb, H.; McBride, C. Not for all: Barriers to universal accessibility in nature-based tourism and recreation spaces across British Columbia, Canada. *J. Outdoor Recreat. Tour.* **2024**, *47*, 100772. [CrossRef]
2. Miller, A.B.; Blahna, D.J.; Morse, W.C.; Leung, Y.-F.; Rowland, M.M. From recreation ecology to a recreation ecosystem: A framework accounting for social-ecological systems. *J. Outdoor Recreat. Tour.* **2022**, *38*, 100455. [CrossRef]
3. Morse, W.C.; Stern, M.J.; Blahna, D.J.; Stein, T. Recreation as a transformative experience: Synthesizing the literature on outdoor recreation and recreation ecosystem services into a systems framework. *J. Outdoor Recreat. Tour.* **2022**, *38*, 100492. [CrossRef]
4. Pellaton, R.; Lellei-Kovács, E.; Báldi, A. Cultural ecosystem services in European grasslands: A systematic review of threats. *Ambio* **2022**, *51*, 2462–2477. [CrossRef]
5. Chen, Y.; Wang, Y.; Zhang, Y.; Luan, Q.; Chen, X. Flash floods, land-use change, and risk dynamics in mountainous tourist areas: A case study of the Yesanpo Scenic Area, Beijing, China. *Int. J. Disaster Risk Reduct.* **2020**, *50*, 101873. [CrossRef]
6. Zhang, Y.; Wang, Y.; Chen, Y.; Xu, Y.; Zhang, G.; Lin, Q.; Luo, R. Projection of changes in flash flood occurrence under climate change at tourist attractions. *J. Hydrol.* **2021**, *595*, 126039. [CrossRef]
7. Paracchini, M.L.; Zulian, G.; Kopperoinen, L.; Maes, J.; Schägner, J.P.; Termansen, M.; Zandersen, M.; Perez-Soba, M.; Scholefield, P.A.; Bidoglio, G. Mapping cultural ecosystem services: A framework to assess the potential for outdoor recreation across the EU. *Ecol. Indic.* **2014**, *45*, 371–385. [CrossRef]
8. Koppen, G.; Ode Sang, Å.; Tveit, M.S. Managing the potential for outdoor recreation: Adequate mapping and measuring of accessibility to urban recreational landscapes. *Urban For. Urban Green.* **2014**, *13*, 71–83. [CrossRef]
9. Cardoso, A.S.; Renna, F.; Moreno-Llorca, R.; Alcaraz-Segura, D.; Tabik, S.; Ladle, R.J.; Vaz, A.S. Classifying the content of social media images to support cultural ecosystem service assessments using deep learning models. *Ecosyst. Serv.* **2022**, *54*, 101410. [CrossRef]
10. Ghasemi, M.; Charrahy, Z.; González-García, A. Mapping cultural ecosystem services provision: An integrated model of recreation and ecotourism opportunities. *Land Use Policy* **2023**, *131*, 106732. [CrossRef]
11. Hooftman, D.A.P.; Ridding, L.E.; Redhead, J.W.; Willcock, S. National scale mapping of supply and demand for recreational ecosystem services. *Ecol. Indic.* **2023**, *154*, 110779. [CrossRef]
12. Inácio, M.; Gomes, E.; Bogdzevič, K.; Kalinauskas, M.; Zhao, W.; Pereira, P. Mapping and assessing coastal recreation cultural ecosystem services supply, flow, and demand in Lithuania. *J. Environ. Manag.* **2022**, *323*, 116175. [CrossRef]
13. Lingua, F.; Coops, N.C.; Griess, V.C. Assessing forest recreational potential from social media data and remote sensing technologies data. *Ecol. Indic.* **2023**, *149*, 110165. [CrossRef]
14. Nyelele, C.; Keske, C.; Chung, M.G.; Guo, H.; Egoh, B.N. Using social media data and machine learning to map recreational ecosystem services. *Ecol. Indic.* **2023**, *154*, 110606. [CrossRef]
15. Fang, L.; Zhang, Z.; Huang, J. Rapid flood modelling using HAND-FFA-SRC coupled approach and social media-based geodata in a coastal Chinese watershed. *Environ. Model. Softw.* **2023**, *170*, 105862. [CrossRef]
16. Ghasemi, M.; González-García, A.; Charrahy, Z.; Serrao-Neumann, S. Utilizing supply-demand bundles in Nature-based Recreation offers insights into specific strategies for sustainable tourism management. *Sci. Total Environ.* **2024**, *922*, 171185. [CrossRef]
17. Guo, R.; Diehl, J.A.; Zhang, R.; Wang, H. Spatial equity of urban parks from the perspective of recreational opportunities and recreational environment quality: A case study in Singapore. *Landsc. Urban Plan.* **2024**, *247*, 105065. [CrossRef]

18. Kang, X.; Qi, J.; Bai, Z.; Xu, W.; Kong, X. Integrating heterogeneous user-generated contents into spatial modeling of agricultural landscape recreational services: A geographically weighted random forest approach. *Ecol. Inform.* **2026**, *96*, 103796. [CrossRef]
19. Shang, N.; Cao, K. Spatial assessment of tourists' demand for cultural ecosystem services in the Kalajun World Natural Heritage Site, China. *J. Outdoor Recreat. Tour.* **2025**, *52*, 100972. [CrossRef]
20. Sokolova, M.V.; Pedes, F.; Fath, B.D.; Romano, S.; Viccaro, M.; Sirca, C.; Spano, D.; Cozzi, M. Integrating citizen science and spatial machine learning for mapping recreational cultural ecosystem services in rural regions. *J. Environ. Manag.* **2026**, *414*, 130405. [CrossRef]
21. Sun, X.; Liu, H.; Liao, C.; Nong, H.; Yang, P. Understanding recreational ecosystem service supply-demand mismatch and social groups' preferences: Implications for urban–rural planning. *Landsc. Urban Plan.* **2024**, *241*, 104903. [CrossRef]
22. Tang, R.; Hou, G.; Chen, Y.; Liu, X.; Chu, S.; Li, L. Spatial and temporal characteristics and driving mechanisms of recreational ecosystem services supply-demand mismatch in rapidly urbanizing areas: Evidence from the Yangtze River Delta. *Ecol. Indic.* **2025**, *171*, 113153. [CrossRef]
23. Wang, Z.; Sun, X.; Shan, R.; Wang, B. Mapping and assessing supply–demand matching of recreational ecosystem services in Shandong province, China. *Ecol. Indic.* **2024**, *160*, 111859. [CrossRef]
24. Hu, Q.; Xiang, L.; Lin, A.; Hou, Y.; Dai, Y. Exploring the spatial configuration of tourism resources through ecosystem services and ethnic minority villages. *Ecol. Inform.* **2024**, *79*, 102426. [CrossRef]
25. Aristizabal, F.; Chegini, T.; Petrochenkov, G.; Salas, F.; Judge, J. Effects of high-quality elevation data and explanatory variables on the accuracy of flood inundation mapping via Height Above Nearest Drainage. *Hydrol. Earth Syst. Sci.* **2024**, *28*, 1287–1315. [CrossRef]
26. Garousi-Nejad, I.; Tarboton, D.G.; Aboutalebi, M.; Torres-Rua, A.F. Terrain analysis enhancements to the Height Above Nearest Drainage flood inundation mapping method. *Water Resour. Res.* **2019**, *55*, 7983–8009. [CrossRef]
27. Nobre, A.D.; Cuartas, L.A.; Hodnett, M.; Rennó, C.D.; Rodrigues, G.; Silveira, A.; Waterloo, M.; Saleska, S. Height Above the Nearest Drainage—A hydrologically relevant new terrain model. *J. Hydrol.* **2011**, *404*, 13–29. [CrossRef]
28. Sabeh, H.; Abdallah, C.; Chahinian, N.; Tournoud, M.-G.; Hdeib, R.; Moussa, R. Evaluating terrain-based HAND-SRC flood mapping model in low-relief rural plains using high resolution topography and crowdsourced data. *J. Hydrol.* **2025**, *652*, 132649. [CrossRef]
29. Thalakkottukara, N.T.; Thomas, J.; Watkins, M.K.; Holland, B.C.; Oommen, T.; Grover, H. Suitability of the height above nearest drainage (HAND) model for flood inundation mapping in data-scarce regions: A comparative analysis with hydrodynamic models. *Earth Sci. Inform.* **2024**, *17*, 1907–1921. [CrossRef]
30. Costache, R.; Tin, T.T.; Arabameri, A.; Crăciun, A.; Ajin, R.S.; Costache, I.; Islam, A.R.M.T.; Abba, S.I.; Sahana, M.; Avand, M.; et al. Flash-flood hazard using deep learning based on H2O R package and fuzzy-multicriteria decision-making analysis. *J. Hydrol.* **2022**, *609*, 127747. [CrossRef]
31. Karmokar, S. Addressing inconsistencies in the El-Shamy's method (1992) in prediction of flash flood susceptibility of the watersheds: A new proposal. *J. Hydrol.* **2025**, *661*, 133710. [CrossRef]
32. Wang, R.; Chen, Y.; Wu, H.; Liu, J.; Wang, M.; Duan, J. A flood susceptibility prediction method for climate change scenarios driven by coupled land simulation and spatiotemporal dual convolution synergy. *J. Hydrol.* **2026**, *664*, 134366. [CrossRef]
33. Wang, Z.; Lyu, H.; Zhang, C. Urban pluvial flood susceptibility mapping based on a novel explainable machine learning model with synchronous enhancement of fitting capability and explainability. *J. Hydrol.* **2024**, *642*, 131903. [CrossRef]
34. Zhuang, Y.; Gong, T.; Fang, J.; Shen, D.; Tang, W.; Lin, S.; Chen, X.; Zhang, Y. Integrating social media data and machine learning methods for flash flood susceptibility mapping in China. *J. Hydrol.* **2026**, *664*, 134397. [CrossRef]
35. Geng, Y.; Huang, X.; Zhong, Y.; Wang, Z. The impact of complex terrain on urban flood resilience under extreme rainfall events. *J. Hydrol.* **2025**, *651*, 132597. [CrossRef]
36. Huang, Y.-F.; Tsang, Y. Unveiling how rainfall spatial structure and displacement drive peak flow magnitude and onset in small mountainous watersheds. *J. Hydrol.* **2025**, *662*, 134069. [CrossRef]
37. Journée, M.; Goudenhoofdt, E.; Vannitsem, S.; Delobbe, L. Quantitative rainfall analysis of the 2021 mid-July flood event in Belgium. *Hydrol. Earth Syst. Sci.* **2023**, *27*, 3169–3189. [CrossRef]
38. Meyer, J.; Neuper, M.; Mathias, L.; Zehe, E.; Pfister, L. Atmospheric conditions favouring extreme precipitation and flash floods in temperate regions of Europe. *Hydrol. Earth Syst. Sci.* **2022**, *26*, 6163–6183. [CrossRef]
39. Wang, L.; Dai, X.; Wang, G.; Yinglan, A.; Miao, C.; Xue, B.; Wang, Y.; Zhu, Y. Establishment of a slope-scale innovated rainfall-runoff model by combining infiltration equation and motion wave equation for watershed flash flood risk prediction. *J. Hydrol.* **2025**, *652*, 132700. [CrossRef]
40. Zoccatelli, D.; Borga, M.; Viglione, A.; Chirico, G.B.; Blöschl, G. Spatial moments of catchment rainfall: Rainfall spatial organisation, basin morphology, and flood response. *Hydrol. Earth Syst. Sci.* **2011**, *15*, 3767–3783. [CrossRef]
41. Fan, Y.; Ma, S. Integrating fuzzy analytic hierarchy process into ecosystem service-based spatial planning: A case study of the Shenyang metropolitan area, China. *Ecol. Inform.* **2024**, *81*, 102625. [CrossRef]

42. Shao, Y.; Xiao, Y.; Kou, X.; Sang, W. Sustainable land use scenarios generated by optimizing ecosystem distribution based on temporal and spatial patterns of ecosystem services in the southern China hilly region. *Ecol. Inform.* **2023**, *78*, 102275. [CrossRef]
43. Wang, P.; Zhang, J.; Ma, J.; Guo, L.; Yang, L.; Ma, X.; Sun, F.; Cao, S. What impacts ecosystem services in tropical coastal tourism cities? A comparative case study of Haikou and Sanya, China. *J. Environ. Manag.* **2023**, *342*, 118227. [CrossRef]
44. Wang, X.; Xiong, J.; Wang, J.; Liu, M.; Zhang, J. Spatiotemporal evolution and driving factors of tourism ecological adaptation in the Dongting Lake Area, China. *Ecol. Inform.* **2024**, *80*, 102459. [CrossRef]
45. Yang, L.; Cao, K. Cultural Ecosystem Services Research Progress and Future Prospects: A Review. *Sustainability* **2022**, *14*, 11845. [CrossRef]
46. Guo, H.; Tian, Y.; Li, J.; Guo, C.; Meng, X.; Wang, W.; De Maeyer, P. Has IMERG_V07 improved the precision of precipitation retrieval in mainland China compared to IMERG_V06? *Remote Sens.* **2024**, *16*, 2671. [CrossRef]
47. Yang, J.; Huang, X. The 30 m annual land cover dataset and its dynamics in China from 1990 to 2019. *Earth Syst. Sci. Data* **2021**, *13*, 3907–3925. [CrossRef]
48. Ross, C.W.; Prihodko, L.; Anchang, J.; Kumar, S.; Ji, W.; Hanan, N.P. HYSOGs250m, global gridded hydrologic soil groups for curve-number-based runoff modeling. *Sci. Data* **2018**, *5*, 180091. [CrossRef]
49. Yamazaki, D.; Ikeshima, D.; Sosa, J.; Bates, P.D.; Allen, G.H.; Pavelsky, T.M. MERIT Hydro: A high-resolution global hydrography map based on latest topography dataset. *Water Resour. Res.* **2019**, *55*, 5053–5073. [CrossRef]
50. USDA Natural Resources Conservation Service. *National Engineering Handbook, Part 630 Hydrology, Chapter 9: Hydrologic Soil-Cover Complexes*; U.S. Department of Agriculture, Natural Resources Conservation Service: Washington, DC, USA, 2004.
51. Moreira, L.L.; Vanelli, F.M.; Schwamback, D.; Kobiyama, M.; de Brito, M.M. Sensitivity analysis of indicator weights for the construction of flood vulnerability indexes: A participatory approach. *Front. Water* **2023**, *5*, 970469. [CrossRef]
52. Li, C.; Liang, Q.; Lin, B.; Zhai, J. Landscape management and planning as a spatial organization method connecting CES supply-demand assessment and sustainable tourism development. *J. Outdoor Recreat. Tour.* **2023**, *44*, 100705. [CrossRef]

Disclaimer/Publisher's Note: The statements, opinions and data contained in all publications are solely those of the individual author(s) and contributor(s) and not of MDPI and/or the editor(s). MDPI and/or the editor(s) disclaim responsibility for any injury to people or property resulting from any ideas, methods, instructions or products referred to in the content.